AIAA-2025-3394

Wall-Bound Streamwise Vortices formed by Embedded Jets in a Turbulent Boundary Layer

Barnabas Toth[1], Bojan Vukasinovic[2] and Ari Glezer[3]
Georgia Institute of Technology, Atlanta, GA 30332-0405

Matthew C. DeFore[4] and Chris Harris[5]
Northrop Grumman Aeronautics Systems

The interactions of a pair of adjacent rectangular wall jets having the same orifice with the inner layer of a flat plate turbulent boundary layer are investigated in wind tunnel experiments in which the characteristic length scales of the yawed jets' orifices are an order of magnitude smaller than the boundary layer thickness. In the present investigations, specific emphasis is placed on the effects of the primary and relative jet yaw angles within the range $45° < \beta < 75°$ and on their relative mass flow coefficients $0.1 < C_q < 0.25$. It is shown that while the interactions of each wall jet with the embedding boundary layer results in the formation of a surface-bound, single-sign vortex, the streamwise evolution of the vortex pair depends on the spanwise positions of the yawed jets relative to the direction of the free stream. The spanwise interactions of the jet-induced vortices are strongly dependent on the jets relative yaw angles, resulting in varied topologies that range from a fully coalesced single vortex to a pair of weakly interacting vortices. It is also shown that the interaction of the two jets can lead to a nearly uniform spanwise momentum flux recovery that within the present parameter range is up to 50% of the boundary layer momentum flux deficit at 100 equivalent orifice diameters downstream from the jets' orifices, and that the net momentum flux gain varies linearly with the relative jets C_q.

Nomenclature

C_q	=	mass flow rate coefficient
U_0	=	freestream velocity
d_e, d	=	(equivalent) jet diameter
Q	=	axial volumetric flowrate
TKE	=	turbulent kinetic energy
U	=	mean streamwise velocity
x	=	direction along the surface
y	=	direction normal to the surface
z	=	direction across the surface span
y	=	direction normal to the surface
β	=	jet yaw orientation
Γ	=	circulation
Δ	=	jet spacing
δ	=	boundary layer thickness
δ^*	=	BL displacement thickness
θ	=	BL momentum thickness
ρ_0	=	free stream density
φ	=	through-plane momentum flux
φ_θ	=	through-plane momentum flux deficit
ω_x	=	streamwise vorticity component

1 Graduate Research Assistant, AIAA Member.
2 Research Engineer, AIAA Member.
3 Professor, AIAA Fellow.
4 Sr. Engineer, AIAA & INPSI Member.
5 Technology Development.

I. Introduction

Jets in cross flow are ubiquitous in a broad range of applications and have been studied extensively in numerous configurations over the years (e.g., Margason, 1993). The classical and most thoroughly studied example of jets in crossflow is the transverse jet, issuing normal and aligned in the direction of the cross flow where the boundary layer interaction with the jet results in the formation of a pair of counter-rotating vortices along the spanwise edges of the jet. Early investigations of the flow were motivated by atmospheric mixing, but they have rapidly evolved to include flows related to species mixing, cooling, aerodynamic maneuvering, etc., as outlined in detailed review articles by Mahesh (2013), Karagozian (2014), and Sharmishtha and Utpal (2017).

The use of circular surface jets for boundary layer control has been of specific interest in various aerospace applications and has been explored in several configurations over the last decades. Motivated by interest to utilize jets in cross flows as 'active' vortex generators in boundary layers over solid surfaces, Johnston and Nishi (1990) used surface-inclined jets for the deliberate formation of streamwise vortices of prescribed sense. They produced configurations of co- and counter-rotating vortices by using inclined surface actuation jets that are yawed relative to the direction of the cross flow and noted the effect of jet yaw on delaying separation. In a review of vortex generator jets, Johnston (1999) noted that strong, single-sense vortices are formed by inclined jets at pitch angles below 45° that are yawed within 60° and 90°. In a later study, Milanovic and Zaman (2003) measured the flow downstream of highly inclined jets in a flat plate boundary layer over a range of yaw and pitch angles, jet momentum ratio and boundary layer thickness and characterized the peak streamwise vorticity, noting that highly yawed jets remain closer to the surface, enhance the turbulence intensity within the boundary layer, and reach their peak vorticity farther downstream.

In contrast to the circular jet, the jets in crossflow out of rectangular orifices have been studied less. Most of the early work, reviewed by Gutmark and Grinstein (1999), was motivated by mixing enhancement and the jet dynamics at the orifice vicinity. Motivated specifically by boundary layer flow applications and streamwise vortex generation, Zhang (2000) considered pitch of 30° and yaw varying from 0° to 135° that resulted in vortices exceeding the boundary layer height while their cores were contained within. He has shown that, in comparison, rectangular jet can produce a stronger vortex than one with a circular orifice for a yaw of 90°. At the same time, the yaw of the rectangular jet yielding the highest circulation was considered to be around 75°, although somewhat dependent on downstream position.

Initial jet-array studies also started with considerations of transverse jets, and Sterland and Hollingsworth (1975) observed the effect of circular jet spacing in cross flow for transverse jets, noting that penetration into the crossflow increases with decreasing jet spacing. A number of investigations focused on arrays of jets in the 1990's was commonly motivated by film cooling applications. Berger and Liburdy (1998) considered compound jet orifices having the exit path diffused either laterally or in pitch. Their results demonstrated that increasing lateral/yaw diffusion results in the flow structures that are well defined and remain close to the surface. Findlay et al. (1999) examined the flow in the wake of 30° inclined rectangular jets, and yaw angle set to 0° and 90°. They found that the latter, spanwise injections generate far greater flow blockage, and that if the jet spacing is small, $s/A = 3$ where A is width of jet orifice, it can prevent the formation of vortices when combined with a high blowing ratio. An array of inclined and swept jets also generates co-rotating vortices, with their merging behavior most commonly characterized by a/b, the ratio of their core size and center to center distance. With some variation, multiple studies indicate that the critical

merging ratio is about $a/b = 0.3$, above which the vortex pair becomes unstable and rapidly combines into a single vortex, though the structure after the merging is elliptical in shape (Cerretelli and Williamson, 2003).

While many aspects of the evolution of inclined yawed jets in cross flow have been investigated and are still investigated due to the large design space, few prior investigations considered the evolution and interaction of such jets within a turbulent boundary layer that has a characteristic scale that is significantly larger than the scale of the jet. The present investigations build on earlier studies by Toth et al. (2024, 2025) that specifically focused on the interactions of pitched and yawed jets with a nominally 2-D cross flow over a flat plate such that the resulting jet-induced vortical structures remain bounded within the inner domain of the turbulent boundary layer. In those prior studies, both circular and rectangular *single* jets have been assessed with various inclinations and yaw angles, and it has been shown that low-inclined rectangular jets offer the greatest momentum gain for the same flow rate, as well as higher circulation within the generated vortex bounds. The present work extends those single-jet studies by considering interactions of a pair of rectangular wall jets within the turbulent boundary layer flow, including the ramifications on the jet-induced gain and redistribution of the boundary layer momentum flux.

II Experimental Setup and Flow Diagnostics

The present investigations are conducted in an open-return, low-speed wind tunnel (Figure 1a) driven by a 150 HP blower (up to 95,000 CFM) with a 10:1 contraction downstream of a turbulence management section having a square test section measuring 106 cm on the side and 304 cm in length. The bottom wall of the test section was replaced with a horizontal flat plate model that can be translated vertically. The tunnel's test section is optically transparent from three sides to enable optical measurements using PIV and flow visualization. Prior to the installation of the flat plate model, the flow uniformity across the tunnel's test section was verified using Pitot probe measurements over a square grid at a range of crosswind speeds. The flat plate model is fabricated from a monolithic composite having a honeycomb core, sandwiched between two aluminum plates. The plate spans the full width of the tunnel's test section and is designed to be mounted so that it splits the airflow downstream of the contraction (Figure 1a) to form a spanwise-uniform boundary layer over its upper surface downstream of a bullnose half cylinder leading edge. The plate is attached on its lower surface to a light aluminum frame connected to four electric risers to enable adjustment of its elevation and streamwise inclination within the test section. Although in the present experiments the plate orientation is horizontal (zero pressure gradient), it is also possible to accommodate small favorable and adverse streamwise pressure gradients. The plate incorporates an opening that is matched

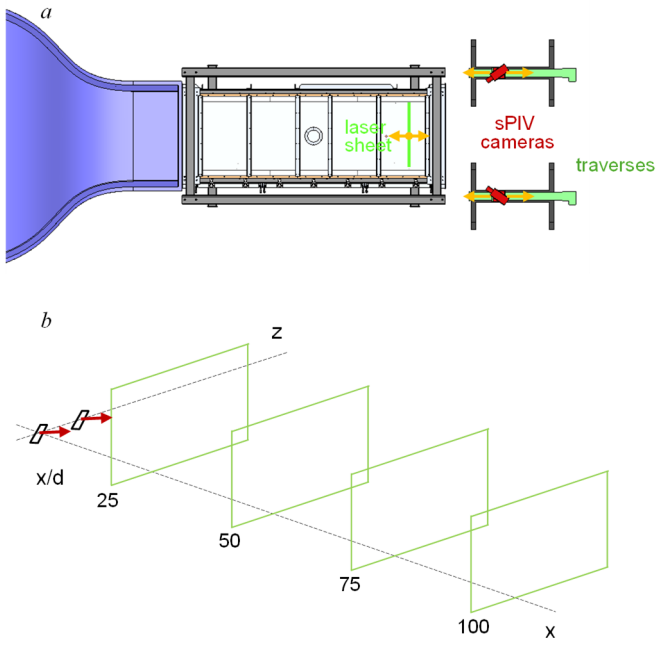

Figure 1. *Top view of schematics of the experimental setup (a), and the sPIV measurement planes (b).*

with the interchangeable module housing jet arrays. In the present experiments the module houses five jet components, where each component is of cylindrical body flush mounted in a liner array across the test section span. In the present investigation, stereo PIV (sPIV) measurements are acquired in the four streamwise-normal *y-z* planes x/d_e = 25, 50, 75 and 100 (relative to the center of the jet orifice), and the nominal PIV optical setup and the measurement planes are schematically shown in Figure 1. The jet orifice center ($x_0 = 0$), is set approximately 1,400d_e away from the leading edge of the plate. In all measurement planes, the spatial vector-resolution of the flow field is kept at about 0.8d_e, where d_e is the equivalent orifice diameter, which will be labeled just as d for the remainder of the paper for simplicity.

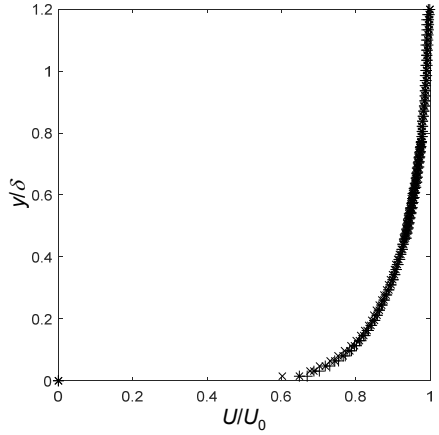

Figure 2. *Boundary layer mean velocity profiles (a) at x/d = 25 (+), 50 (•), 75 (∗) , and 100 (×).*

Baseline flow is kept fixed in the present experiments at $Re_x = 1.47 \cdot 10^6$ m^{-1}. Prior to experimental investigations of the jet interactions with boundary layer flows, baseline boundary layer was characterized by the sPIV measurements over the two overlapping fields of view to ensure capturing of the free stream. Such measurements were conducted at all four streamwise measurement locations, and the resulting mean boundary layer profiles are shown in Figure 2. While the overlapped profiles indicate a very close agreement, the main characteristic BL parameters indicate a small but consistent growth between x/d = 25 and 100, where $\delta \approx 98 - 108$ mm, $\delta^* \approx 9.9 - 11.2$ mm, and $\theta = 7.1 - 8.1$ mm. Across the four planes, the BL shape factor remains fairly consistent at $h = 1.38$.

As prior work by Toth et al. (2025) has shown that interaction with a rectangular jet with the BL flow can utilize Coanda effect for maintaining the resulting swirling jet downstream evolution in close proximity to the surface, the present investigation expands that study on such jets'

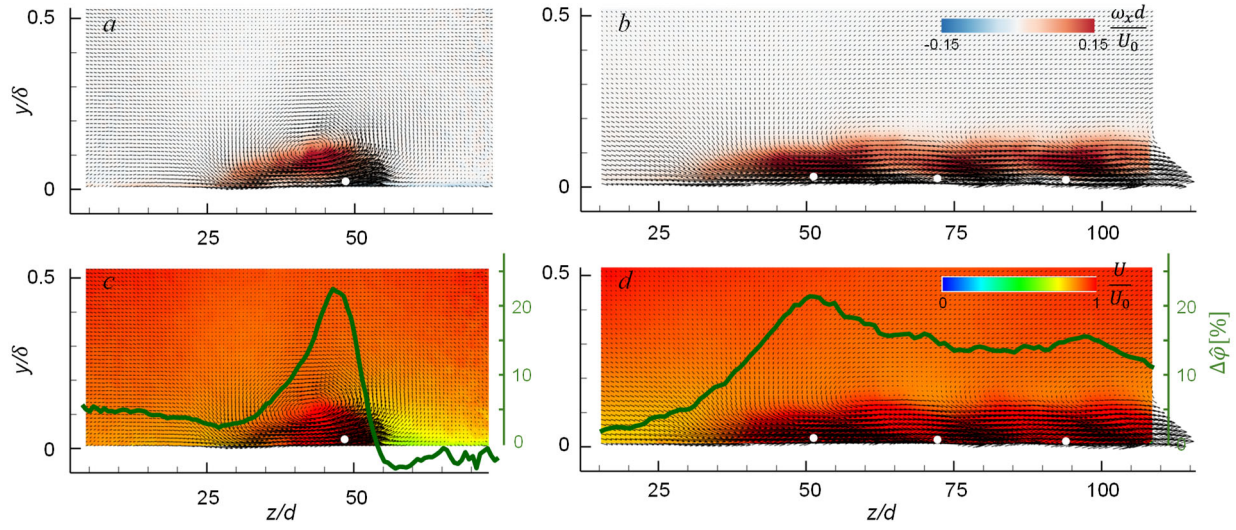

Figure 3. *Color raster plots of the mean streamwise vorticity (a,b) and velocity (c,d) for the single jet (a, c) and five-jet array (b, d) jet interaction with the boundary layer at x/d = 50, and the jets' yaw angle β = 60°. Spanwise distribution of the net momentum change relative to the baseline boundary layer flow is overlaid in (c,d).*

interactions within the turbulent boundary layer, while the jet issues into the flow as a wall jet instead at the pitch $\alpha = 20°$ of the prior study. To illustrate differences between a single and multiple-jet interaction with the boundary layer flow, Figure 3 shows the upstream view of the resulting flow composition at $x/d = 50$ downstream from the jet issuance at the pitch and yaw ($\alpha = 20°$, $\beta = 60°$). A single-jet mean vorticity is shown in Figure 3a, while the raster plot of the mean streamwise velocity component, with overlaid in-plane mean velocity vectors is shown in Figure 3c. Similar to the single-jet results by Toth et al. (2025), the resulting mean-flow streamwise vortical structure adheres close to the surface (Figure 3a), while providing the highest velocity increment at the domain of the largest velocity deficit of the boundary layer (Figure 3c). However, this net contribution to the BL velocity momentum is not only localized about the vortex structure. Distribution of the net change in the resulting flow momentum across the measured flow span is overlaid in Figure 3c, indicating two characteristic features: there is an extension of the net momentum gain on the downwash side of the vortex, and the net loss on the upwash side. In the case of the vortex strong adherence to the surface, the downwash gain dominates the upwash loss, although not full spanwise extents are captured in this field of view. While only three of the five jets remain visible at $x/d = 50$ for the jet array (Figures 3b and d), both fields indicate a clear interaction between the adjacent jets, where each jet core is marked by a dot. It is reasonable to expect that each of the jets evolutions would depend on whether it interacts only with the outer flow (single) or partially (end jets in array) or fully (inner jets in array) with the adjacent jets as well. Interestingly, all the three captured jets have similar (~52–53d) spanwise deflection, which is higher than the 48d for the single jet. Also, when considering a cumulative momentum flux gain across the span (Figure 3d), a nearly uniform gain is measured across the inner array, having a milder drop-off at the end, while the peak gain is associated with the outmost jet.

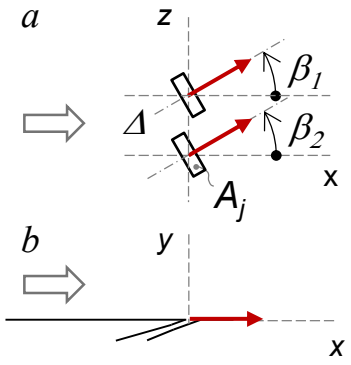

Figure 4. *Top (a) and cross-sectional (b) views of the leading and trailing rectangular wall jets, having the yaw (β_1, β_2) directions marked.*

As illustrated in Figure 3, although the multi-jet interactions and evolution within the boundary layer flow can be guided by the prior study of a single yawed and inclined jet, a better understanding of the interaction mechanisms requires extension of the prior study to multi-jet array. The present study focuses on interactions between two adjacent jets issuing into the boundary layer flow in a close proximity to surface, as shown schematically in Figure 4. The jet-orifice geometry is the same as in the single-jet study by Toth et al (2025), except that the prior pitch angle of $\alpha = 20°$ is further reduced to conform the jet issuance as close to awall jet as geometrically possible. Based on the single-jet evolution, the jet spacing is fixed at about $\Delta = 20d$ to allow adjacent jet interactions within $x/d = 100$.

While the jets' pitch angle α is kept constant and equal for both jets, their yaw relative to the free stream can be independently set, as illustrated in Figure 4a in the top view. Relative to the direction of the jet yaw with respect to the free stream direction, the outer jet in this view is defined as the leading (β_1) and the other one as the trailing (β_2) jet. As already stated above, jet characteristic dimension is defined as its equivalent diameter d_e, which denoted only as d for simplicity. Also, the jet characteristic parameter C_q is defined as the mass flow rate through the jet relative to the mass flow through the boundary layer across the jet's characteristic dimension (per jet), i.e., $C_q =$

$\dot{m}_j/(\rho_0 U_0(\delta - \delta^*)d)$, and it is nominally set to $C_q = 0.2$ for both jets and all studies, except for the unequal jet circulation studies.

III. Boundary Layer Interactions of Yawed Wall Jet Pair

Present investigation considers the three major aspects of the jet pair interactions within the turbulent boundary layer: (*i*) effect of the joint yaw orientation of the jets, where both jets assume the same $\beta = \beta_1 = \beta_2$, (*ii*) effect of the relative yaw orientation between the jets ($\beta_1 \neq \beta_2$), and (*iii*) effect of the unequal jet circulation ($C_{q1} \neq C_{q2}$).

III.1 Equal Yaw Angles

Since the single-jet studies by Toth et al. (2025) indicated a tradeoff between the net added momentum and circulation with the increase in yaw angle, and suggested a rather wide optimum centered at about $\beta = 60°$, and the present investigation focuses on the range of yaw angles $\beta = 45° - 75°$, in increments of $\Delta\beta = 5°$.

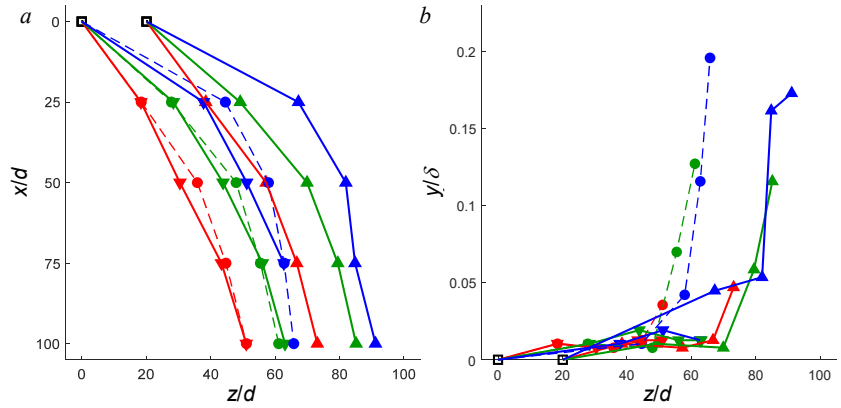

Figure 5. *Spanwise jet deflection with streamwise distance (a) and the deflection away from the surface (b) for the three yaw angles β = 45° (—), 60° (—), and 75° (—), for the single (●), leading (▲), and the trailing (▼) jet.*

Initially, the resulting jet trajectories across four measurement planes (x/d = 25, 50, 75, and 100) are compared among the single and the leading and trailing jets, in a dual jet configuration, where the jet position at any plane is defined by its peak velocity. Figure 5 illustrates both the jet deflection in the spanwise direction, and away from the surface for three yaw orientations, β = 45°, 60°, and 75°. As expected, regardless of which jet is considered, initial sidewise deflection (Figure 5a) increases with the yaw angle, which is followed by the jet trajectory alignment with the free stream (x) direction, although it is noted that even at $x/d = 100$, the jets' trajectories do not appear completely aligned with the free stream. For the dual jets, they initially maintain approximately the same spacing Δ at $x/d = 25$, but with further downstream evolution become spaced farther apart, albeit not significantly. A single jet initially deflects more than the trailing jet (x/d = 25, 50), but as it seems to align earlier with the free stream, this deflection resembles that of the trailing jet by x/d = 75 and 100. In all cases other than $x/d = 25$, the deflection of the leading jet leads both the trailing and single jet. It is interesting to note that both the single and the leading jet follow a similar deflection pattern away from the surface (Figure 5b), as both jets begin to deflect approximately once they reach the sideways displacement of about $50d$. Although deflecting, the jets still remain close to the surface, reaching only about 0.2δ at $x/d = 100$. Contrary to these two jets, the trailing jet adheres to the surface longer, as it will be further discussed later, with no significant displacement through the whole measurement extent, up to $x/d = 100$.

To illustrate how the paired yaw orientation reflects on the BL flow field, Figures 6-1 show velocity fields at the farthest downstream location (x/d = 100) for each of the seven yaw orientations $\beta = \beta_1 = \beta_2 = 45° – 75°$. Besides the progressive vortex pair deflection sidewise with increasing yaw angle, it is more important to note the difference in the evolutions of the leading jet/vortex (in this upstream view on the right) and the trailing one. When comparing the leading jet evolution with an equivalent isolated/single jet (Toth et al., 2025), they both progressively grow in size / gain in circulation, at the expense of a loss in momentum, reflected by the decreasing

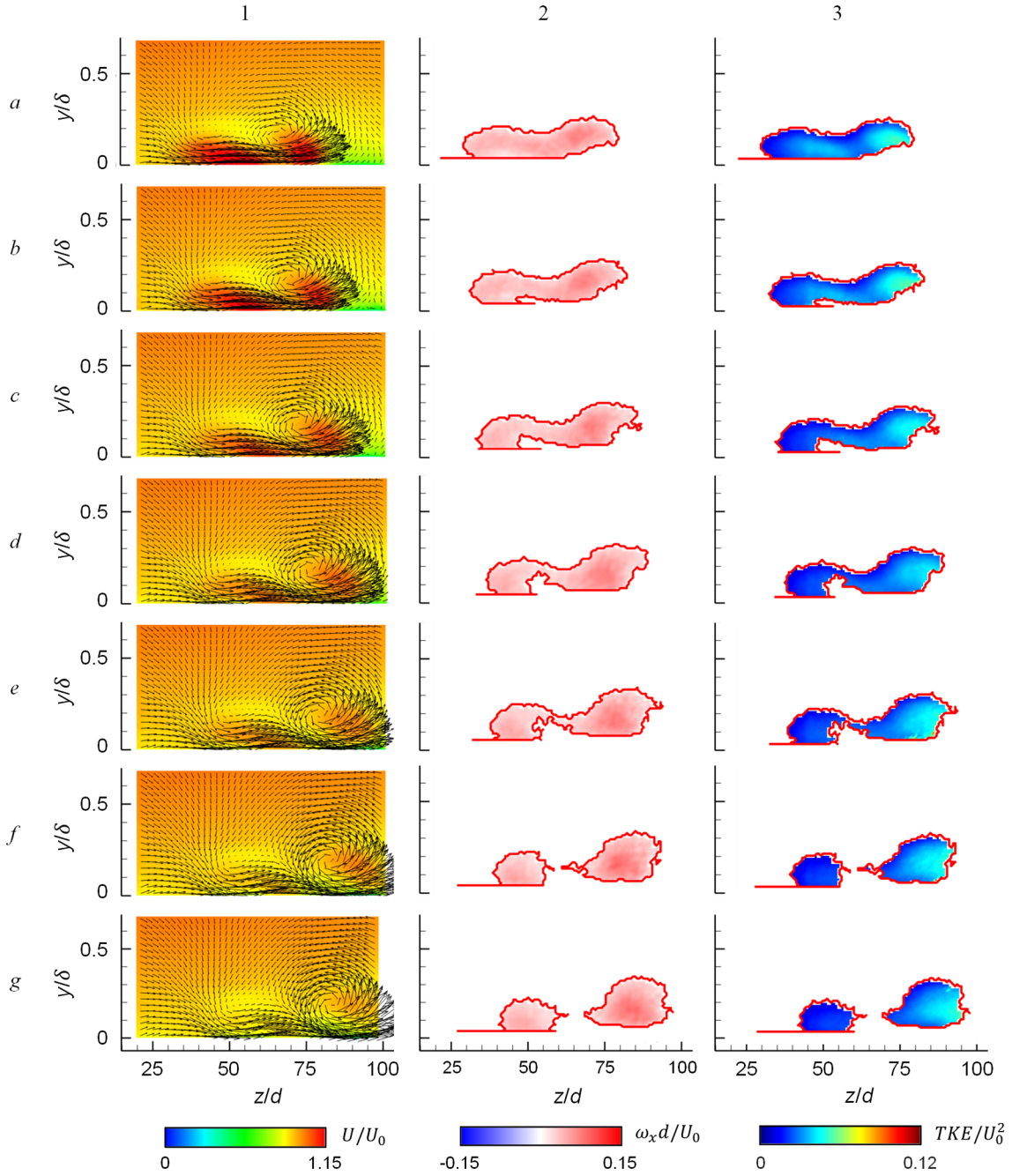

Figure 6. *Color raster plots of the upstream view of mean streamwise velocity with overlaid in-pane mean velocity vectors (1), and vortex-bound mean streamwise vorticity (2) and TKE (3) at x/d = 100 downstream from the jet orifices for the jet pair yaw angles β = 45° (a), 50° (b), 55° (c), 60° (d), 65° (e), 70° (f), and 75° (g).*

streamwise velocity component in Figures 6-1 with increasing β. However, the trailing jet evolution appears to be significantly affected by the presence of the leading jet. Besides the lowest β case (Figure 6-1a), the trailing vortex, in the mean-flow sense, resembles a braid-like structure of the primary vortex, indicating that their interaction likely leads to the trailing vortex being engulfed by the primary one. Although such pairing process is clearly not completed by $x/d = 100$, it may be argued that they may ultimately coalesce farther downstream. While the signature of this trailing vortex also loses momentum with increasing β, it remains in the close proximity to surface in all instances. In addition to the velocity fields, another insight into the flow evolution of the interacting jets/vortices is gained by considering vorticity and turbulent kinetic energy (TKE) distributions within the vortex bounds. As already outlined by Toth et al. (2025), to isolate the evolution of these vorticity concentrations, the Γ_1 criterion (Graftieaux et al. 2001, Berson et al. 2009) is utilized to define the centers and bounds of vorticity concentrations. When applied to the flow fields in Figures 6-1, the embedded vortical structures are isolated, and only the extracted vortex contours are shown, along with raster plots of the mean streamwise vorticity (Figures 6-2) and TKE (Figures 6-3) magnitudes within these bounds. It is noted that the velocity, vorticity, and TKE ranges are fixed in the plots for all the measurement planes, which diminishes the color contrast at $x/d = 100$. Nonetheless, it is seen that not only does the primary vortex grow larger in size, but it also embodies higher vorticity levels, clearly dominating the circulation contribution of the pair. Also, it is seen that the increasing β also increases the vortex separation in the far field. As an indication of the flow unsteadiness and turbulent mixing, contour plots of TKE in Figures 6-3 suggest that the TKE, like vorticity, retains higher levels with the bounds of the leading vortex, relative to the trailing one. These peak levels are associated with the highest shear region of the leading vortex and appear to progressively diminish in magnitude with increasing β, while spreading over the larger portion of the vortex bounds, in line with the mixing and entrainment of the surrounding fluid.

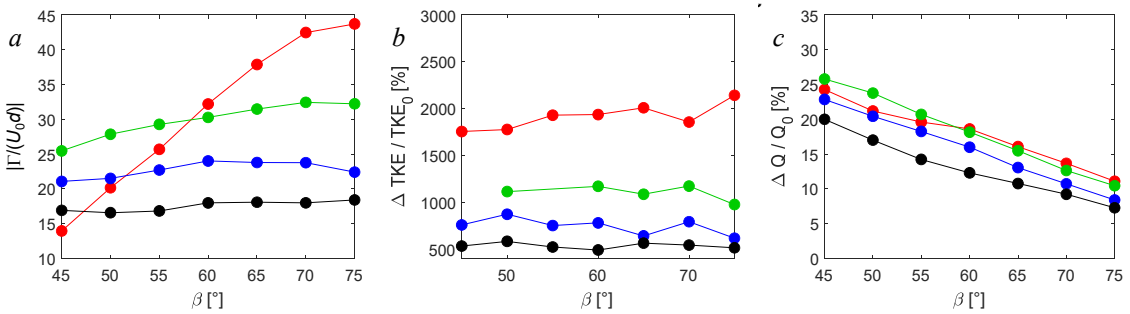

Figure 7. *Circulation (a), and the TKE (b) and volumetric flow rate (c) gain within the vortex bounds for the jet pair yaw angles $\beta = 45° - 75°$ at $x/d = 25$ (●), 50 (●), 75(●), and 100 (●).*

Based on the extracted flow fields like the one shown in Figure 6 for $x/d = 100$, a composite analysis of the vortex descriptors for all the joint yaw orientations, as measured across all four planes, is based on the evolutions of vortex circulations, turbulent kinetic energy, and volumetric flow rate, all within the extracted vortex bounds, shown in Figure 7. The generally expected trend of the increasing vortex circulation with β, as it was clearly demonstrated by Toth et al. (2025) for a single jet, is seen for the vortex pair in Figure 7a. The continuing interactions in the downstream direction quickly weaken this relationship, which results in a nearly leveled circulation at $x/d = 100$ in contrast with closer planes. Interestingly, the TKE levels (Figure 7b) appear only weakly dependent on the joint yaw orientation β, while indicating a clear suppression in the downstream

direction, arguably due to the transport and dissipation of the initial high levels of TKE brought about by the jet issuance into the BL. Lastly, Figure 7c indicates that at least in the added axial volumetric flow rate through the vortex bounds, there is a very close agreement between the observations for a single jet (Toth et al., 2025) and dual jets of the present study. It should be noted, though, that the jet-induced flow still turns, in alignment with the outer flow, and that only the streamwise component is considered for its relevance to the boundary layer flow. Through all planes there is a strong decline in the axial flow rate carried within the vortical bounds with increasing β, which can be argued to be a consequence of the increasing losses with the jet issuance at directions increasingly opposing the boundary layer mean-flow direction.

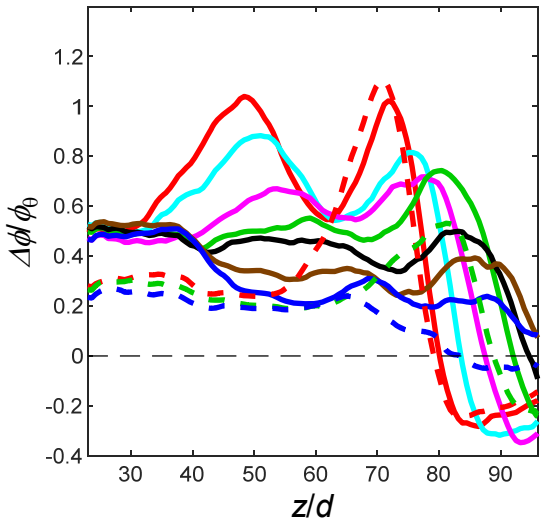

Figure 8. *Distribution of spanwise momentum increment $\Delta\varphi$ relative to the baseline boundary layer momentum deficit φ_θ at x/d = 100 for two jets issuing at equal yaw angles β = 45° (—), 50° (—), 55° (—), 60° (—), β = 65° (—), 70° (—), 75° (—), as well as a single jet at β = 45° (---), 60° (---), and 75° (---).*

Presumably the most important integral measure of the jet/vortex interaction with the turbulent boundary layer is reflected in the added momentum flux, both from the standpoint of its net magnitude and distribution across the span. Hence, the next step is the analysis of the paired yaw angle effect, distributions of the change in the momentum flux across the measured flow span are defined by difference of the linear integrals of the momentum flux of the boundary layer flow in the presence and absence of jet vortices $\Delta\phi$, which is expressed relative to the momentum deficit of the baseline boundary layer flow ϕ_0. Such linear integrals compose spanwise distributions of the relative change shown in Figure 8 at x/d = 100 for all the paired jets. In addition, three equivalent distributions for a single jet case are added for comparison (β = 45°, 60°, and 75°), where the single jet origin is shifted to match the origin of the leading jet of the pair for direct comparison, since similarities in their evolution are already noted earlier. In general, the dual jet interaction shows similar regions of the momentum flux change as in the single jet – the central domain of the peak gain is bound by a weaker net gain that extends on the 'downwash' side of the vortical structures, while there is a weak domain of the net loss in momentum flux on the 'upwash' side of the concentration of vorticity. The dual peak in the net gain is most pronounced for the lowest-yaw pair, having the peak gain decreasing and shifting sideways, with vortex displacement, with the increasing β. While the distribution appears bimodal for the lowest β pair, it levels with the increasing yaw angle up to about β = 65°, where the most uniform distribution is attained, at the gain of about 45% of the momentum deficit of the baseline boundary layer. Clearly, depending on objectives, less uniform but even higher (on average) net gains can be achieved at lower angles, at another tradeoff of the narrower spanwise spread of the effect. Lastly, comparisons with a single jet, which distributions are shown in dashed lines, indicate remarkable similarity with the leading jet distribution for β = 45°, when the least interaction between the leading and trailing jets are noted. Past the single jet, on the downwash side, its extended benefit is expressed through the prolonged gain of about 25% of the baseline deficit, while the presence of the trailing jet seems to

elevate that 'residual' effect to almost 50% (at the lowest z/d). However, for the other two single jet orientations, which correspond to enhanced interactions between the leading and the trailing jets, the net contribution of the single jet is considerably smaller than its leading jet counterpart.

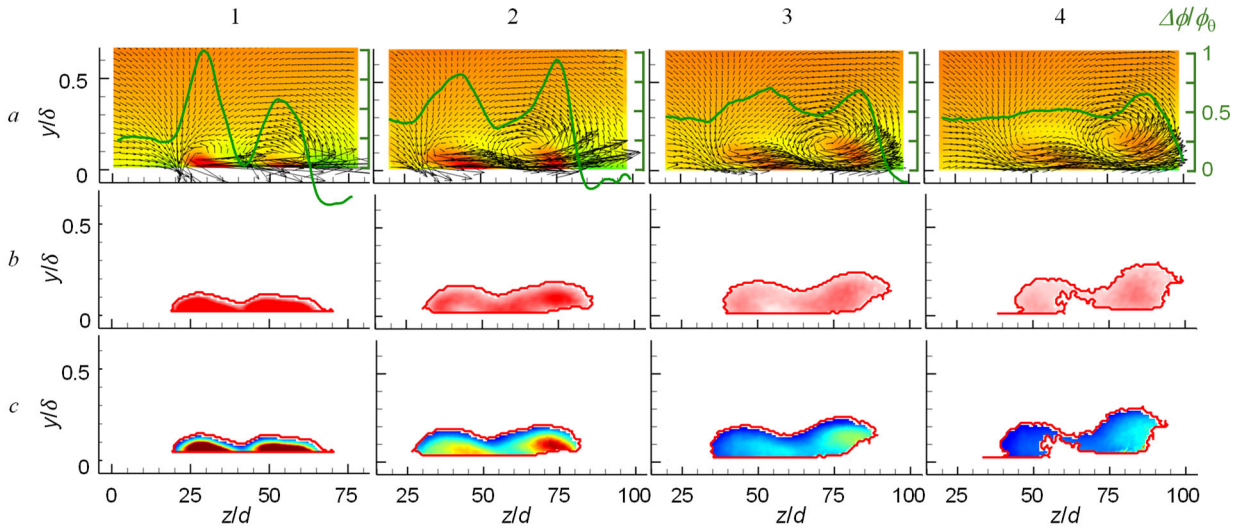

Figure 9. *Color raster plots of the upstream view of mean streamwise velocity with overlaid in-pane mean velocity vectors (a), and vortex-bound mean streamwise vorticity (b) and TKE (c) as in Figure 6, at x/d = 25 (1), 50 (2), 75 (3), 100 (4), downstream from the jet orifices for the jet pair yaw angle β = 65°.*

Although the momentum flux analysis of Figure 8 does not point to a sharp optimum with respect to the maximization of the net momentum flux gain, the joint yaw of $\beta = 65°$ is selected as a good candidate due to its reasonably uniform distribution at $x/d = 100$. Before proceeding with analysis of the jet's relative yaw with respect to this selected $\beta = 65°$, this paired jet evolution is shown in greater detail in Figure 9. Figures 9a show the velocity field evolution through the four measurement planes, along with the overlaid distributions of the net momentum flux change $\Delta\phi/\phi_0$, where ϕ_0 is the boundary layer momentum flux deficit of the base flow. At the most upstream plane (Figure 9a-1), the direct momentum contribution by the jets maintains the dominant double-peak distribution, in this case it is even biased toward the trailing jet, although these two contributions are typically comparable. It is also seen that the upwash-positive and downwash-negative contributions extend on each side of the bimodal gain. At the next measurement plane (Figure 9a-2), the continuing jet-jet interaction and their interaction with the boundary layer spread the central gain across the wider span, favoring the net-positive tail at low z/d and diminishing the net negative effect on the upwash side. As the interaction continues through $x/d = 75$ (Figure 9a-3) and down to $x/d = 100$ (Figure 9a-4), the initial peaks continue to diffuse, improving the distribution uniformity across the span, eventually reaching the reasonably uniform distribution at $x/d = 100$, which was already shown in Figure 8 as well. Similar to the analysis related to Figure 6, vorticity bounds for these four flow realizations are also extracted, and raster plots of vorticity and TKE carried within these bounds are also shown in Figure 9. Characteristic surface-bound vortices induced by initial interaction between the issuing jets and boundary layer flow are isolated at the first measurement plane (Figure 9b-1), indicating similarly high levels of not only the CCW vorticity, but also with respect to the TKE (Figure 9c-1). Already at the next measurement plane (Figures 9-2), an uneven evolution between the leading and trailing jets is noted, with the leading vortex beginning to displace away from the surface. Prevailing vorticity is associated with the leading jet/vortex, which also carries higher levels of TKE. Both vorticity and TKE levels continue

to drop as the vortices grow in the streamwise direction, to the point that, due to very low levels between them, they appear nearly separated at the farthest downstream location (Figures 9-4). Hence, concurrently with the leveling of the net momentum flux across the span at this location, the turbulent mixing and the jet-induced circulation become significantly suppressed.

III.2 Varying Relative Yaw

Once the $\beta = 65°$ is pre-selected as a candidate for further studies of the jets' interactions due to the jets' realized near uniform momentum gain distribution at the farthest downstream distance $x/d = 100$ (cf. Figure 9a-4), it is of interest to force the jets to merge earlier upstream by changing the relative yaw angle between them, instead of issuing them both parallel to each other, at $\beta = 65°$. To facilitate this, the trailing jet is kept fixed at $\beta_2 = 65°$, while the orientation of the leading jet is varied at lower angles $\beta_1 = 25°$, 35°, 45°, and 55°, thereby forcing the jets' interaction upstream from the prior case of $\beta_1 = 65°$. To illustrate the effect of such a change of the relative yaw between the two jets, the resulting flow fields at $x/d = 50$ are shown in Figure 10, including the limit case of $\beta_1 = \beta_2 = 65°$. Although the resulting flow signatures are predictably intermixed, the state of the merger between the two jets for the highest relative yaw angle between the jets (Figures 10a) still yields a somewhat unexpected result. The joint structure closely resembles a single circular jet topology (e.g., Toth et al., 2025) rather than that of a rectangular jet. Only the vortical bounds in Figure 10a-2 indicate a small but present remnant of the primary-jet-induced vortex, while the nearly merged structure is dominated by the trailing vortex. Contrary to this scenario, it was already shown above that during the natural evolution of the vortices having $\beta_1 = \beta_2$, the trailing vortex is the one that becomes engulfed by its primary counterpart. Already at the next shallower relative yaw (Figures 10b), an incomplete interaction between the vortices becomes more pronounced, although the dominance of the trailing vortex still remains, at least relative to its size. Both vortical structures become almost equally compressed to the surface for $\beta_1 = 45°$ (Figures 10c), although vorticity concentrations in Figure 10c-2 suggest a reversal to the dominance of the primary vortex, by its contribution to circulation. At the shallowest relative yaw (Figures 10d), the initial interaction becomes sufficiently delayed, such that the flow structure closely resembles that of zero relative yaw (shown in Figures 10e for reference). In both cases, the primary jet is clearly dominant both in its size and

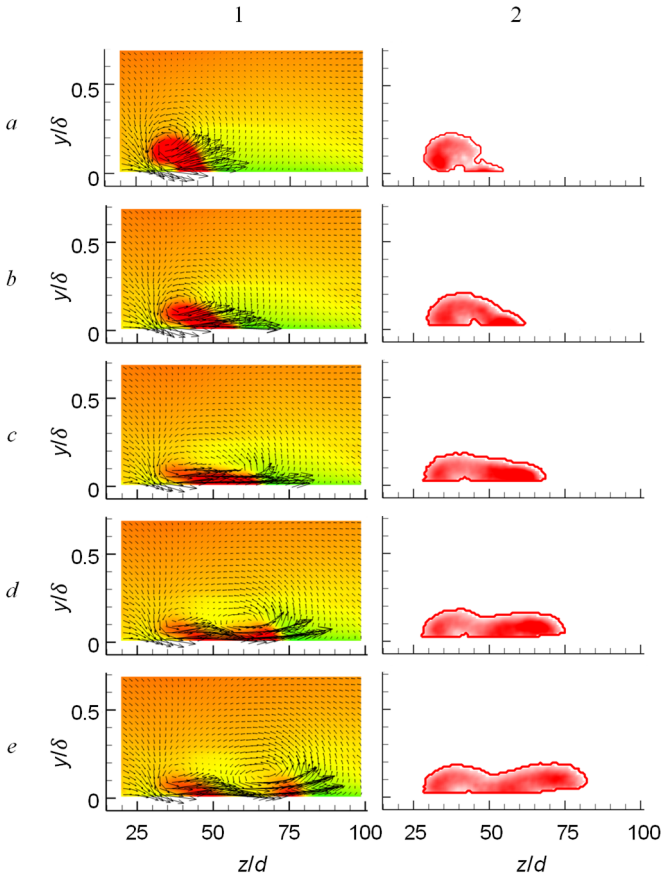

Figure 10. *Color raster plots of the upstream view of mean streamwise velocity with overlaid in-pane mean velocity vectors (1), and vortex-bound mean streamwise vorticity (2) as in Figure 6, at x/d = 50, with the trailing jet $\beta_2 = 65°$, and the leading jet $\beta_1 = 25°$ (a), 35° (b), 45° (c), 55° (d), 65° (e).*

circulation, having the wider spanwise extent for the parallel jets case. In summary, these tests with the varying relative angle between the jets suggest that the streamwise tailoring of the jets' interaction can be done at shallower angles, but the structure of interaction changes at steeper relative angles, resulting in the narrow rounded vortical structures akin to topologies seen in single circular jet interactions with boundary layer flows.

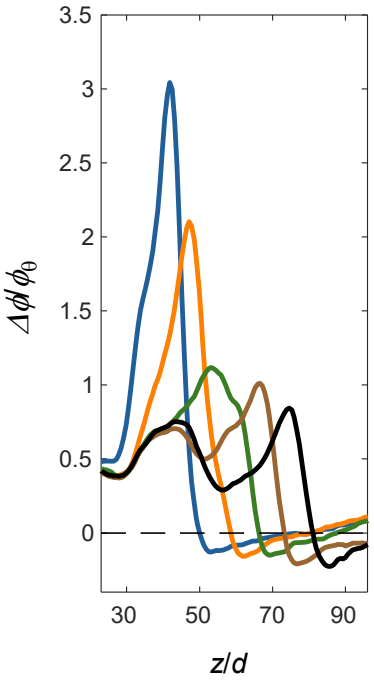

Figure 11. *Distribution of spanwise momentum flux increment $\Delta\varphi$ relative to the baseline boundary layer momentum deficit φ_θ for the cases shown in Figure 10: β_1 = 25° (—), 35° (—), 45° (—), 55° (—), 65° (—).*

The main cumulative indicator of the jet-pair interaction with the boundary layer flow is defined as the net gain in the momentum flux relative to the baseline boundary layer. Analogous to the relative parameter introduced in Figure 8, Figure 11 shows the distributions of $\Delta\phi/\phi_0$ across the measured flow span at x/d = 50 for all the relative yaw angles discussed in Figure 10. Remarkably, forcing the near-field interaction between the jets at the steepest relative yaw (for β_1 = 25°) results in an extremely focused gain in momentum flux, somewhat resembling the effect of a singular round jet at zero yaw (cf. Toth et al, 2025). Therefore, similar to that jet, the impulse-like increase in momentum becomes balanced by an extremely narrow domain of influence. Similar to the single peak distribution seen for β_1 = 25°, the next shallower relative yaw (for β_1 = 35°), still indicates a unified structure, across the domain that is associated with the trailing jet. Only for β_1 = 45°, although at significant drop in the peak gain, the spanwise distribution begins to resemble the dual-jet signature, only largely dominated by the leading jet side. This trend continues as the relative yaw approaches zero (parallel jets at $\beta_1 = \beta_2$ = 65°), with the mild drop in peak gain and progressive spanwise extent on the side of the leading jet. These distributions indicate that a rather wide variety of the two-jet interactions can be tailored by simple adjustments in the nonzero relative yaw between the jets on the order of 10 degrees. In practice, this can be simply facilitated by a rotary motor controlling the azimuthal orientation of individual cylindrical jet module.

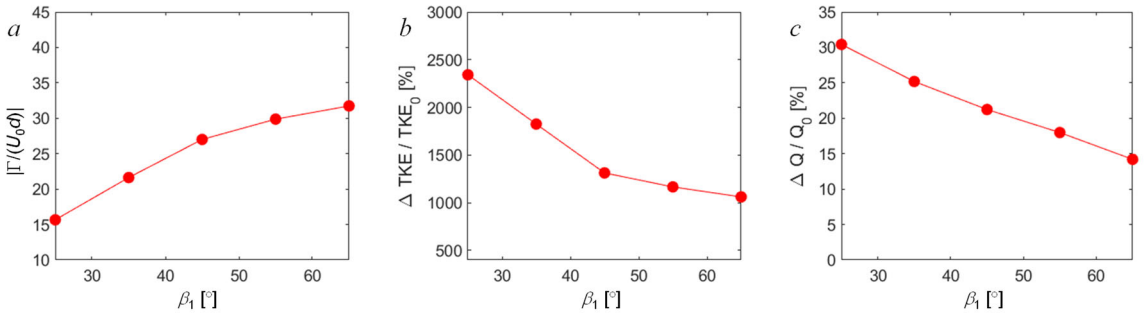

Figure 12. *Circulation (a), and the net change of TKE (b) and volumetric flow rate (c) within the vortex bounds for the cases shown in Figure 10.*

Further quantification of the overall effects of the yaw relative angle is done by calculations of the resulting circulation, TKE, and the volumetric flow rate within the vortex bounds for the same cases discussed with respect to Figures 10 and 11. As it can be expected, when the jets interaction is forced in the upstream direction by increasing the relative yaw angle between the jets, their circulation decreases at the fixed downstream location x/d = 50, as seen in Figure 12a. This outcome is equivalent to the circulation decrease in the downstream direction for the fixed yaw orientations of the jets. Simultaneous drop in the relative TKE contribution with reduction in the relative yaw angle (down to zero at β_1 = 65°), seen in Figure 12b, results also from delaying the jets' interactions toward and even past the measurement plane at x/d = 50 with increasing β_1. Again, this finding is in accord with the TKE decrease in the downstream direction, as discussed in connection with Figure 9. Interestingly, the upstream initiation of the jets interactions does increase the volumetric flow rate gain carried within the vortex bounds, increasing it from about $\Delta Q/Q_0$ = 15% at β_1 = 65° to about 30% at β_1 = 25° (Figure 12c). Such an increase is likely connected to the earlier flow alignment with the free stream, increasing the streamwise component of velocity within the vortex bounds.

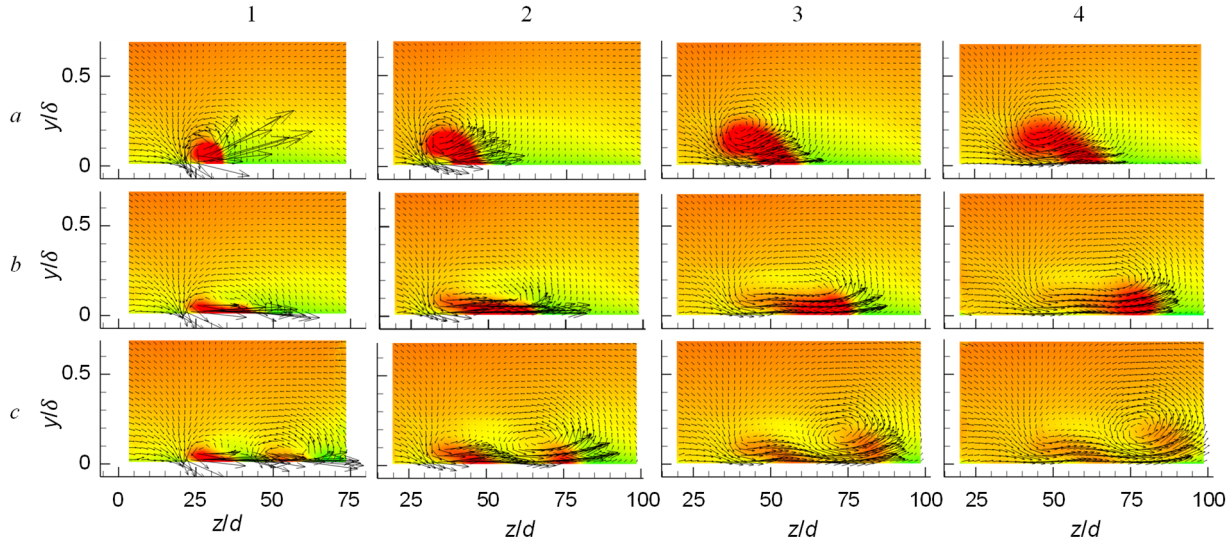

Figure 13. *Color raster plots of the upstream view of mean streamwise velocity with overlaid in-pane mean velocity vectors as in Figure 6, at x/d = 25 (1), 50 (2), 75 (3), and 100 (4) with the trailing jet β_2 = 65°, and the leading jet β_1 = 25° (a), 45° (b), 65° (c).*

A closer look at the variety of flow interactions that result from small changes in the relative yaw is taken for three disparate tested angles of the leading jet, β_1 = 25°, 45°, and 65°, where the full flow field evolution through the four measured cross-stream planes at x/d = 25, 50, 75, and 100 is shown in Figure 13. Despite the noted similarity for the sharpest relative yaw (β_1 = 25°) in terms of the resulting joint vortical structure at x/d = 50 (Figure 10a-1) and that of a single round jet (Toth et al., 2025), the full downstream evolution for the dual jet (Figures 13a) points to a major difference. While the round jet-induced vortex drifts away from the surface in the downstream direction, the joint vortical structure of the two merged jets persistently adheres to the surface in the downstream direction, while increasing in size due to entrainment. The next possible flow realization is illustrated for the shallower jets' interaction in Figures 13b (β_1 = 45°). It is interesting that a joint structure appears to be the most evenly spread across the span, where none of its constituting vortices resembles a fully coherent structure in the mean. Similar to the downstream evolution for β_1 = 25°, the initially formed structure at x/d = 25 (Figure 13b-1), progressively

grows in the downstream direction, while adhering to the surface. The only noted difference is that the peak velocity gain gradually shifts to the leading jet side. Lastly, for reference, the limit state of the zero relative yaw is replicated in Figures 13c. This flow evolution was already discussed in connection with Figures 9a, and here mostly serves to illustrate a breadth of the possible flow outcomes. In this case, no complete jet merger is noted at any of the planes. Nonetheless, it was shown that such 'incomplete' interaction arguably results in the most favorable momentum flux gain (cf. Figure 9a-4).

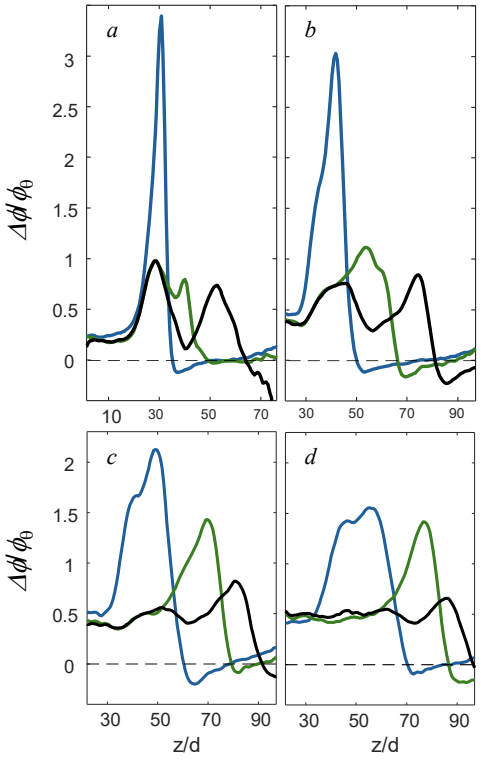

Figure 14. *Distribution of spanwise momentum flux increment $\Delta\varphi$ relative to the baseline boundary layer momentum deficit φ_θ at x/d = 25 (a), 50 (b), 75 (c) and 100 (d), with the trailing jet $\beta_2 = 65°$, and the leading jet $\beta_1 = 25°$ (—), 45° (—), and 65° (—).*

Since the initial assessment of the relative yaw angle influence of the momentum flux gain (cf. Figure 11), indicated a rather wide spectra of distributions, it is of further interest to examine the downstream evolution of the net momentum change for the three characteristic cases discussed in Figure 13. Therefore, Figure 14 shows the corresponding net momentum changes at all the four measurement stations. The most important result is seen in that the upstream wide disparity between the steep and shallow relative yaw interactions (Figures 14a and b), subsides farther downstream (Figures 14c and d). Hence, it appears that the sharp, pulse-like gain for the steep relative yaw spatially diminishes faster than those of the other two relative orientations, such that the peak distributions, at least for $\beta_1 = 25°$ and 45°, are comparable at $x/d = 100$ (Figure 14d). While the zero relative yaw case clearly results in the most uniform distribution at that last plane, it would be of interest to further assess the 'asymptotic' states for the other two interactions farther downstream, since their distributions at $x/d = 100$ suggest that the momentum flux transfer across the span is not completed. This finding might be counterintuitive, as it suggests that by forcing the upstream jet interactions (by adjusting the relative yaw), the resulting momentum flux transfer across the span (ideally close to uniform) becomes prolonged when compared to the initial interaction commencing at downstream location. This is certainly at least partially attributed to the fact that the jets do not completely coalesce in the case of the zero relative yaw. Still, this finding suggests that the forced strong interaction between adjacent jets results in a prolonged distribution of momentum across the span due to its narrow focusing across the unified vortical structure.

III.3 Unequal Jet Momentum

After the relative jet-pair yaw considerations in Section III.2, the jets' configuration that resulted in the most 'flattened' vorticity distribution was deemed of interest by the perceived most uniform contribution of the excess velocity/momentum across the span and along the surface (Figures 13b). This configuration, having the leading jet yaw orientation ta $\beta_1 = 45°$ and the trailing jet oriented at $\beta_2 = 65°$, is further examined by altering the balance in the jets' 'strengths', facilitated by the

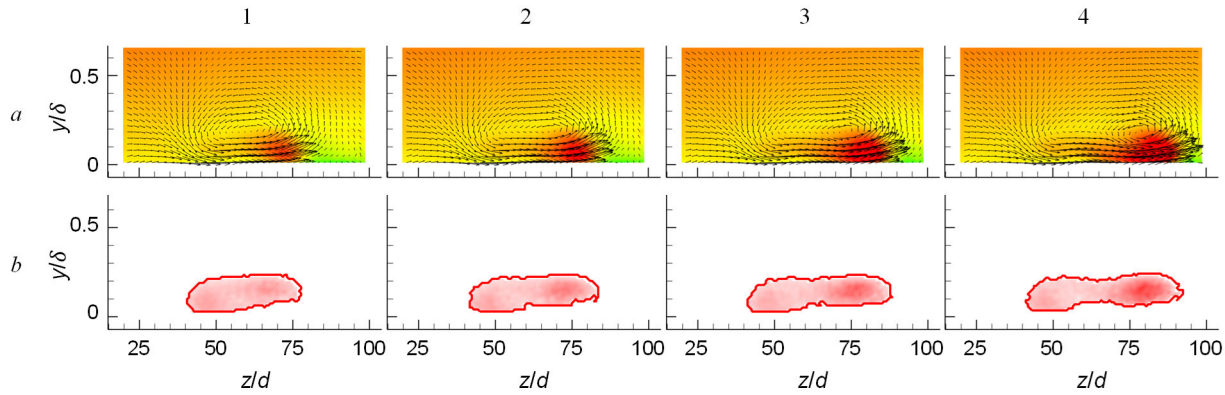

Figure 15. *Color raster plots of the upstream view of mean streamwise velocity with overlaid in-pane mean velocity vectors (a), and vortex-bound mean streamwise vorticity (b) as in Figure 6 at x/d = 100 with the trailing jet C_q = 0.2 at β_2 = 65° and the leading jet at β_1 = 45°, C_q = 0.1 (1), 0.15 (2), 0.2 (3) and 0.25 (4).*

change in the jet C_q parameter, which essentially alters the jet-induced circulation. Therefore, the jets orientations are kept fixed during this study, along with the trailing jet C_{q2} = 0.2, while the leading jet parameter is varied as C_{q1} = 0.1, 0.15, 0.2, and 0.25. The resulting mean velocity flow fields are shown in Figures 15a, while the corresponding mean streamwise vorticity is shown within the extracted vortex bounds in Figures 15b. Just as the jet parameter becomes progressively increased, it is seen that the joint vortical structure at the last measurement plane also progressively extends spanwise. It can be argued that the increased C_{q1} facilitates prolonged initial deflection of the leading jet, which likely somewhat prolongs initial interaction with the trailing jet, thereby extending the compound domain of influence. It is also noted that, with increasing C_q, the primary vortex structure becomes more pronounced, especially at the highest C_{q1} = 0.25 (Figure 15a-4). In addition, a featureless distribution of vorticity for the lowest C_{q1} (Figure 15b-1) gradually gives a rise to the single-pole high vorticity domain on the side of the leading vortex, even when the leading jet has lower or equal C_q than the trailing one.

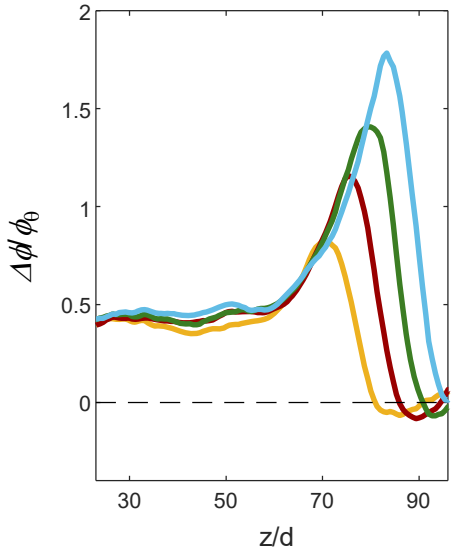

Figure 16. *Distribution of spanwise momentum flux increment Δφ relative to the baseline boundary layer momentum deficit φ_θ at x/d = 100 with the trailing jet C_{q2} = 0.2 at β_2 = 65° and the leading jet β_1 = 45° issuing with C_{q1} = 0.1 (—) 0.15 (—) 0.2 (—) and (0.25) (—).*

The proportional flow response to the varying primary jet parameter C_{q1} is also clearly reflected in distributions of the net relative momentum flux gain, as shown in Figure 16 for all the cases considered in Figure 15. The primary jet effect remains confined only on its side, where the net momentum flux gain both extends sideways and elevates in magnitude, while the gain on the trailing jet side remains virtually unchanged and even, just below 50% of the base flow momentum flux deficit. Hence, similar to the changes in the relative yaw angle, it is possible to extend the spanwise reach of the jet-pair momentum flux increase (by also prolonging the downstream evolution) by simple adjustment of uneven jet parameters. However, Figure 16 suggests that attaining that this by varying C_{q1} instead of the yaw

angle β_l eliminates the need for moving parts and also easily correlates the net gain of momentum flux with the jet parameter.

VI. Conclusions

Interactions between a flat plate turbulent boundary layer ($Re_x = O[10^6]$) and a pair of adjacent wall jets issuing from the plate surface were investigated in wind tunnel experiments. The yaw angles of the wall jets relative to the free stream could be independently varied and the characteristic scale measured by the equivalent diameter $d = d_e$ of their identical rectangular orifices was about an order of magnitude smaller than boundary layer thickness. The present investigations focused primarily on the effects of primary and relative jet yaw angles within the range $45° < \beta < 75°$ and on their relative mass flow coefficients $0.1 < C_q < 0.25$, where C_q is defined as a ratio of the jet mass flow rate to the mass flow rate within the boundary layer across the jet's characteristic scale. The evolution of the flow field near the surface in the absence and presence of the jets was measured using stereo PIV in streamwise-normal planes at four streamwise locations $x/d = 25$, 50, 75, and 100 downstream from the jet orifices.

Similar to the findings of Toth et al. (2025), it is shown that the interactions of each wall jet with the inner boundary layer results in the formation of a surface-bound, single-sign vortex that remains in close proximity to the surface as it is advected downstream. The present investigations showed that the evolution of the vortex formed by each wall jet of an adjacent jet pair having the same yaw angles depends on the spanwise position of the yawed jet relative to the free stream. The first and second jet relative to the direction of the yaw is termed the leading and trailing jet, respectively. While the evolution of the leading jet is similar to that of a single jet, the trailing jet typically loses its coherence as it is drawn and become engulfed into the primary vortex associated with the leading jet. This interaction weakens the joint circulation dependence on the common yaw orientation of the jets, while the axial flow carried by the vortices decreases proportionally to β. It was also shown that these yaw interactions between the jets assist in spanwise spreading of concentrated momentum flux by each jet within the inner wall layer resulting in nearly spanwise uniform recovery of up to 50% of the momentum flux deficit in the baseline boundary layer across the measured span, at 100d downstream from the jets orifices.

It was also shown that spanwise interactions of the jet pair depend strongly on their relative yaw angles, resulting in a variety of streamwise topologies that range from a fully coalesced single vortex to a pair of weakly interacting vortices, and enable tailoring of spanwise spreading of momentum flux at some given streamwise distance from the jets' orifices. Changes in the relative yaw angle can force vortex interactions close to the jets' orifices, while the concomitant increase in concentrated streamwise momentum flux can delay and even limit spanwise uniformity of the gain in momentum flux compared to the evolution of two jets with the same yaw angles. Finally, it was also shown that for given yaw angles the spanwise distributions of streamwise momentum recovery can be adjusted by the relative mass fluxes of the leading and trailing jets.

Acknowledgment/Disclaimer

This work was sponsored by the Office of Naval Research (ONR), under grant number N000142312500. The views and conclusions contained herein are those of the authors only and should not be interpreted as representing those of ONR, the U.S. Navy, or the U.S. Government. The authors also want to acknowledge assistance of Dr. Derek Nichols with some data post-processing tools and procedures.

References

Berger, P. A. and Liburdy, J. A., "A Near-Field Investigation into the Effects of Geometry and Compound Angle on the Flowfield of a Row of Film Cooling Holes," ASME Paper 98-GT-279, 1998.

Berson, A., Michard, M., and Blanc-Benon, P., "Vortex identification and tracking in unsteady flows," *Comptes Rendus Mécanique,* Vol. 337, No. 2, 2009, pp. 61-67.

Cerretelli, C., and Williamson, C. H. K., "The physical mechanism for vortex merging," *Journal of Fluid Mechanics*, Vol. 475, 2003, pp. 41–77.

Findlay, M. J., Salcudean, M., and Gartshore, I. S., "Jets in a crossflow: Effects of geometry and blowing ratio," *Journal of Fluids Engineering*, Vol. 121, No. 2, 1999, pp. 373–378.

Graftieaux, L., Michard, M., and Grosjean, N., "Combining PIV, POD and vortex identification algorithms for the study of unsteady turbulent swirling flows," *Measurement Science and Technology,* Vol. 12, No. 9, 2001, pp. 1422-1429.

Gutmark, E. J., and Grinstein, F. F., "Flow Control with Noncircular Jets," *Annual Review of Fluid Mechanics*, Vol. 31, 1999, pp. 239–272.

Johnston, J., and Nishi, M., Vortex generator jets – means for flow separation control, *AIAA Journal,* Vol. 28, 1990, pp. 989–994.

Johnston, J.P. "Pitched and Skewed Vortex Generator Jets for Control of Turbulent Boundary Layer Separation: A Review," Proceedings of the 3rd ASME/JSME Joint Fluids Engineering Conference, FEDSM99-6917, 1999.

Karagozian, A.R., "The Jet in Crossflow," *Physics of Fluids*, Vol. 26, No. 10, 2014, pp.1-47.

Mahesh, K., "The Interaction of Jets with Crossflow," *Annual Review of Fluid Mechanics*, Vol. 45, 2013, pp. 379-407.

Margason, R. J., "Fifty Years of Jet in Crossflow Research," In Computational and Experimental Assessment of Jets in Cross Flow, *AGARD-CP-534*, 1993.

Milanovic, I.M. and Zaman, K. B. M. Q. "Fluid Dynamics of Highly Pitched and Yawed Jets in Crossflow," *AIAA Journal*, Vol. 42, No. 5, 2024, pp. 874 - 882.

Sharmishtha, C. and Utpal, B., "Review of Jets in a Cross Flow-Experimental and Numerical Approach," *International Journal of Engineering and Advanced Technology*, Vol. 7, No. 2, 2017, pp. 114-128.

Sterland, P. R. and Hollingsworth, M. A., "An Experimental Study of Multiple Jets Directed Normally to a Cross-Flow," *Journal of Mechanical Engineering Science*, Vol. 17, No. 3, 1975, pp. 117-124.

Toth, B., Vukasinovic, B., Glezer, A., DeFore, M.C., and Harris, C., "Interactions of Controlled Streamwise Vortices with a Turbulent Boundary Layer," AIAA Paper 2025-1489, 2025.

Toth, B., Nichols, D. A., Vukasinovic, B., and Glezer, A., DeFore, M.C., and Harris, C., "The Evolution of Streamwise Vortices Formed by Inclined and Swept Round Jet within a Turbulent Boundary Layer," AIAA Paper 2024-3634, 2024.

Zhang, X. "An Inclined Rectangular Jet in a Turbulent Boundary Layer—Vortex Flow," *Experiments in Fluids*, Vol. 28, 2000, pp. 344–354.